Langmuir

Article

pubs.acs.org/Langmuir

Gravity-Driven Hybrid Membrane for Oleophobic–Superhydrophilic Oil–Water Separation and Water Purification by Graphene

Hyun Yoon,[†] Seung-Heon Na,[†] Jae-Young Choi,[†] Sanjay S. Latthe,[†] Mark T. Swihart,[‡] Salem S. Al-Deyab,[§] and Sam S. Yoon*[,†]

[†]School of Mechanical Engineering, Korea University, Seoul 136-713, Republic of Korea

[‡]Department of Chemistry & Biological Engineering, University at Buffalo (SUNY), Buffalo, New York 14260, United States

[§]Petrochemicals Research Chair, Department of Chemistry, College of Science, King Saud University, Riyadh 11451, Saudi Arabia

Supporting Information

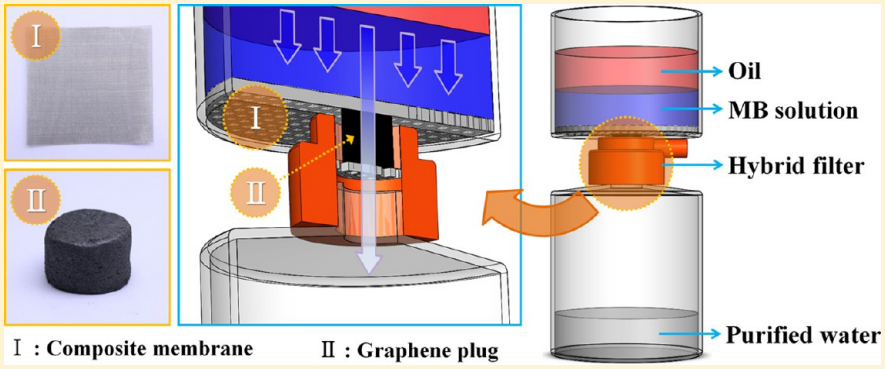

ABSTRACT: We prepared a simple, low-cost membrane suitable for gravity-driven oil–water separation and water purification. Composite membranes with selective wettability were fabricated from a mixture of aqueous poly(diallyldimethylammonium chloride) solution, sodium perfluorooctanoate, and silica nanoparticles. Simply dip-coating a stainless steel mesh using this mixture produced the oil–water separator. The contact angles (CAs) of hexadecane and water on the prepared composite membranes were 95 ± 2° and 0°, respectively, showing the oleophobicity and superhydrophilicity of the membrane. In addition, a graphene plug was stacked below the membrane to remove water-soluble organics by adsorption. As a result, this multifunctional device not only separates hexadecane from water, but also purifies water by the permeation of the separated water through the graphene plug. Here, methylene blue (MB) was removed as a demonstration. Membranes were characterized by high-resolution scanning electron microscopy (HRSEM), transmission electron microscopy (TEM), X-ray photoelectron spectroscopy (XPS), and Fourier transform infrared (FT-IR) spectroscopy to elucidate the origin of their selective wettability.

1. INTRODUCTION

The creation of efficient adsorbent materials and membranes for the separation and removal of oils and organic pollutants from water remains important in addressing environmental issues.[1,2] The economic and environmental concerns surrounding oil spills have motivated investigations of numerous oil–water separation materials, such as inorganic porous materials (for example, clay, talc, calcium fly ash, zeolites, silica aerogel)[3,4] and organic biodegradable materials (for example, straw, hull, corncob, peat moss, sugar cane bagasse, wood/cotton fibers, wool-based materials).[5−9] Traditional techniques for oil–water separation such as air flotation, gravity separation combined skimming, oil-adsorbing materials, coagulation and flocculation, and others[10−12] are restricted by low separation efficiency, high energy input, and complex separation steps. A major challenge is the fabrication of a functional material that can perform efficient oil–water separation at a low cost, with high selectivity, and that can also be produced on a large scale in an environmentally friendly manner and be easily recycled.[13]

Surfaces exhibiting extreme wetting behavior, namely superrepellency and superwetting, have generated immense industrial and academic interest. Materials with special wettability have been designed for oil–water separation. These functional materials either filter or adsorb oils or water from mixtures selectively.[14−18] However, the use of superhydrophobic–superoleophilic membranes requires considerable energy because water tends to form a barrier layer between the oil and the hydrophobic surface during the separation process owing to the higher density of water than of the most oils, which in turn prevents the permeation of oil through the membrane. Even during an oil removal process, these membranes are easily fouled by the adhered or adsorbed oils, especially high-viscosity oils, because of their intrinsic oleophilic nature. Difficulty in cleaning and reusing such membranes results in secondary pollution.[19−21] In contrast, superoleophobic–superhydrophilic materials, owing

Received: March 30, 2014

   dx.doi.org/10.1021/la5031526 | Langmuir XXXX, XXX, XXX−XXX

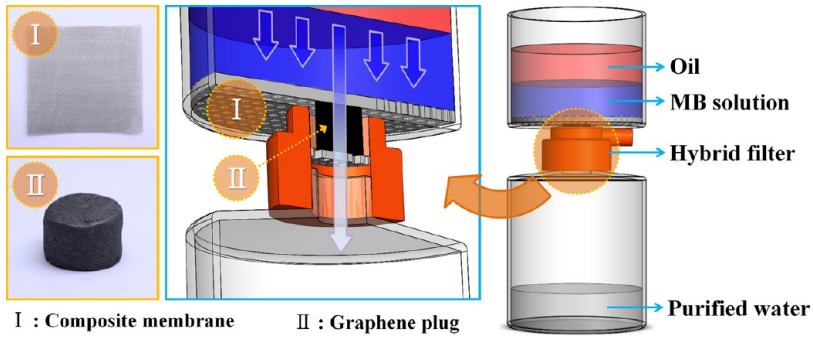

Figure 1. Efficient oil–aqueous MB separation as well as water purification, where a hybrid filter contains a graphene plug (see image II) below the hydrophilic/oleophobic composite membrane (see image I).

to their high separation efficiency, resistance to oil fouling, and easy recyclability, can provide a practical means of oil–water separation.[22] When a mixture of oil and water is put on a superoleophobic–superhydrophilic membrane, oil will stay on the upper part of the membrane, and the water will penetrate through the membrane and be collected below.

An ideal superoleophobic surface is demonstrated by some sea animals such as fish and sharks, whose skin can effectively repel oil while being wetted by water to function as self-cleaning surfaces.[23,24] The self-cleaning mechanism of fish skin can be attributed to the interaction between the surface hydrophilic mucus and the presence of multiscale structures. Fish scales show a hierarchical structure consisting of sectorlike scales with diameters of 4–5 mm covered by papillae 100–300 μm in length and 30–40 μm in width. Encouraged by the properties of fish scales, artificial superoleophobic–superhydrophilic surfaces have been prepared in recent years, and the study of surface oil wettability is growing as a research focus in materials science.

Liu et al.[25] found that surfaces that are both hydrophilic and oleophilic, when separately exposed to water or oil under air, can exhibit oleophobic character in water. As a result, oil contaminants are washed away when immersed in water. Yang et al.[26] fabricated a superhydrophilic and superoleophobic composite coating by spray casting SiO_2 nanoparticle complex polymer suspensions on various substrates. Recently, Zhang et al.[27] described an approach that uses a block copolymer comprised of pH-responsive poly(2-vinylpyridine) and oleophilic/hydrophobic polydimethylsiloxane blocks to functionalize materials, including nonwoven textiles and polyurethane sponges, to prepare surfaces with switchable superoleophilicity and superoleophobicity in aqueous media. Xue et al.[22] fabricated a superhydrophilic and underwater superoleophobic polyacrylamide (PAM) hydrogel-coated mesh at a three-phase oil/water/solid interface. It could selectively separate water from oil–water mixtures with a high separation efficiency and resistance to oil fouling, and it was easily recycled.

Graphene, a two-dimensional structure consisting of sp^2-hybridized carbon, has stimulated increasing interest in the field of materials science over the past decade. The unique properties of graphene were discovered by Novoselov et al., who thoroughly described the wide range of its potential physical, chemical, biological, photoelectric, and catalytic applications.[28] Graphene-based materials have been studied and applied for the adsorption of organic pollutants such as dyes, polycyclic aromatic hydrocarbons, and gasoline. Graphene can provide a large specific surface area for the adsorption of organic molecules.[29]

2. EXPERIMENTAL SECTION

2.1. Nanocomposite Membrane. We stacked graphene flakes (which formed a bulk graphene "plug") below the composite membrane. Optical microscope images of the graphene plug are shown in Figure S1. The multifunctional device not only separated a hexadecane and aqueous methylene blue (MB) mixture, but also removed MB completely during the separation. The overall features of our membrane are described in Figure 1. As illustrated there, this simple "one-step" membrane is assembled from stainless steel meshes coated with polymer–silica mixtures, and a graphene plug which adsorbs impurities, removing model pollutants. Because this membrane is relatively simple and inexpensive to produce, such membranes may enable practical portable and efficient oil–water separators and water purifiers in industrial wastewater treatment and oil spill cleanups.

2.2. Materials. Silica nanoparticles (SiO_2, 99.5%), poly(diallyldimethylammonium chloride) solution (PDDA, $(C_8H_{16}ClN)_n$, 20 wt % in H_2O), MB, and hexadecane ($CH_3(CH_2)_{14}CH_3$) were purchased from Sigma-Aldrich in Korea. Ethyl alcohol (CH_3CH_2OH; 99.9%) was purchased from Duksan Chemical in Korea. Oil Red O ($C_{26}H_{24}N_4O$) and sodium perfluorooctanoate (PFO, $C_8F_{15}O_2Na$, 97%) were purchased from Alfa Aesar in Korea. Multilayered graphene flakes were purchased from XG Sciences (Lansing, MI). More details of the graphene flakes are available in Table 1. The graphene flakes had an

Table 1. Typical Properties of Graphene Nanoplatelets

property [unit]	typical value	
	parallel to surface	perpendicular to surface
density [g/cm^3]	2.2	2.2
carbon content [%]	>99.5	>99.5
thermal conductivity [W/m·K]	3000	6
thermal expansion [m/m/deg.·K]	4–6 × 10^{-6}	0.5–1.0 × 10^{-6}
tensile modulus [GPa]	1000	na
Tensile strength [GPa]	5	na
electrical conductivity [S/m]	10^7	10^2

average diameter and thickness of 25 μm and 6–8 nm, respectively, a surface area of 120–150 m^2/g, and an oxygen content of less than 1%. Stainless steel meshes used as substrates (pore size ranging from ~42 to 60 μm) were purchased from Hyundai Fence Steel Mesh. Double distilled deionized (DI) water was used for rinsing, dilution, and other purposes to avoid any impurities in the final products.

2.3. Synthesis of the Oleophobic–Superhydrophilic Composite Membranes. The dip-coating technique is not restricted to any particular type of substrate. Hence, the oleophobic–superhydrophilic composite coating can be applied to various substrates such as metal, glass, paper, or fabrics without any special surface treatment. Here, the stainless steel meshes were cleaned by rinsing with absolute ethanol and acetone before dip coating. First, PDDA aqueous solution (7.2 mL), PFO powder (1.75 g), and SiO_2 nanoparticles (50 mg) were mixed under continuous and vigorous stirring at ambient temperature. A highly

dx.doi.org/10.1021/la5031526 | Langmuir XXXX, XXX, XXX–XXX

viscous slurry was formed after approximately 5 min of vigorous stirring. The rotation rate of the stirrer was 600−800 rpm. This chemical composition of the slurry, hereafter called PP-SiO_2, was kept constant throughout the series of experiments. Second, 1 g of the above-mentioned PP-SiO_2 was added to ethanol under vigorous stirring. The resulting final slurry solution was used to coat the stainless steel meshes by dip-coating which lasted for 10 s duration. These prepared composite membranes were dried under atmospheric conditions for 24 h to completely evaporate the solvent. One gram of PP-SiO_2 was added separately to varying amounts of ethanol (2.5, 3.8, 5.1, and 6.3 mL). The composite membranes (CM) prepared with 2.5, 3.8, 5.1, and 6.3 mL of ethanol were named as CM-1, CM-2, CM-3, and CM-4, respectively. Note that the viscosity of the slurry solution comprising both SiO_2 and ethanol was measured in the range of 11.8 ± 0.2 cP for CM-1, which yielded the best oil−water separation. A slight fluctuation in the value was due to the slurry nature of the fluid containing SiO_2 nanoparticles.

2.4. Characterization of the Oleophobic−Superhydrophilic Membranes. The viscosity of as-prepared precursor was measured using a viscometer (Brookfield model LVDV-I+, Spindle CPE-40). The oleophobic−hydrophilic composite membranes were characterized by high-resolution scanning electron microscopy (HRSEM) (XL30SFEG Philips Co., Netherlands at 10 kV). Their wettability was determined by static contact angle (CA) measurements in air. A goniometer was used to measure and record the static CA on the membranes after a drop of 3 mm in diameter was placed on the membrane at a steady state. DI water was supplied to a stainless-steel nozzle (inner and outer diameters of 100 and 240 μm, respectively) via a syringe pump (KDS Legato 100) at a flow rate of 0.4 mL/min. All measurements and experiments were performed under ambient conditions. The average static CA value was obtained from measurements from at least five fresh positions on the same sample. A high-speed camera (Vision Research, Inc., Phantom 7.3) was used to capture the CA images on the prepared oleophobic−hydrophilic membranes. The oil−water separation experiment with the oleophobic−hydrophilic composite membranes was performed by fixing the membrane between two beakers. The effective diameter of the membrane was 18 mm, through which water passed. A 150 mL mixture of hexadecane and water (v/v: 50/100 mL) was poured onto the composite membrane, and the liquid was collected in a beaker below. Separation was achieved under gravity. The oleophobic−super-hydrophilic composite membranes were also evaluated in terms of the separation from oil and decolorization of the MB solution, which was prepared with 1.12 g of MB (whose initial concentration was 3×10^{-2} mol) and 100 g of D.I. water. MB is a model dye for wastewater of the dyeing industry.[30] The graphene-plug had a diameter and thickness of 21 and 20 mm, respectively, and had weight of 3.9 g and density of 1.13 g/cm^3; see image II in Figure 1. The graphene plug was made by simply squeezing graphene flakes into the top cylinder of the "Hybrid filter" indicated in Figure 1. The optical absorption in the spectral region of 300−800 nm was assessed using a UV−vis spectrophotometer (Optizen POP Mecasys Co. LTD).

3. RESULTS AND DISCUSSION

3.1. Surface Morphology of the Composite Membranes. Figure 2 shows the composite membrane, CM-1, synthesized on the stainless steel mesh using the highest concentration solution in ethanol. Figure 2a shows an HRSEM image of the stainless steel mesh with an average square-shaped pore size ranging from ∼42 to 60 μm. After dip coating, a dense layer of composite coating material was observed on the surface and in the pores of the stainless steel mesh (Figure 2c). Figure 2b shows an optical image of the noncoated and coated parts of the stainless steel mesh.

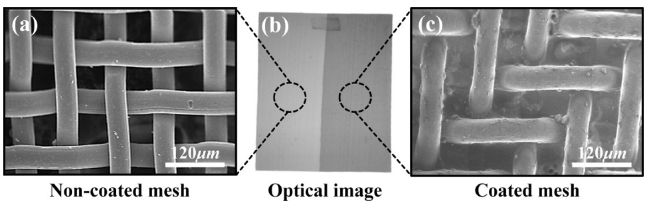

Figure 2. (a) HRSEM image of the stainless steel mesh, (b) optical image of uncoated and composite-coated stainless steel mesh, and (c) HRSEM image of composite-coated stainless steel mesh.

Figure 3 shows comparative HRSEM images of the composite membranes CM-1, CM-2, CM-3, and CM-4. After dip coating,

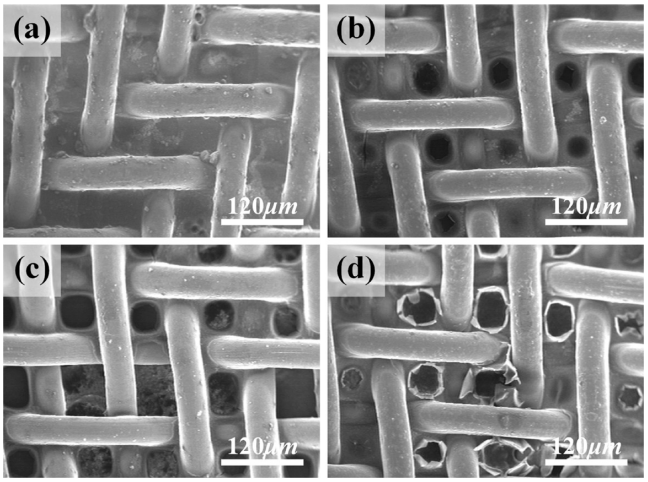

Figure 3. Comparative HRSEM images of composite membranes: (a) CM-1, (b) CM-2, (c) CM-3, and (d) CM-4 in the order of increasing ethanol amount (toward lowering PP-SiO_2 concentration).

CM-1 shows a smooth and dense layer of composite coating material on the micrometer scale stainless steel wires and in the pores of the stainless steel mesh (Figure 3a). The pores were fully and homogeneously covered by the coating material. No visible coating defects or cracks were found on CM-1. This homogeneous membrane was highly reproducible when assembled under the same fabrication conditions; please see Figure S2 in the Supporting Information. We were able to produce the pore structure in a repeatable manner, which was ensured by producing the same pore structure and morphology of at least five different samples produced under the same fabrication conditions; please see Figures S3−S6 in the Supporting Information. In addition, we confirmed reproducibility of our membrane performance by obtaining the same results on different days.

Interestingly, in the case of CM-2 (Figure 3b), we observed some holes with average diameters ranging from ∼5 to 35 μm on the surface of the membrane. In the case of CM-3 (Figure 3c) and CM-4 (Figure 3d), these holes were larger. The coating material deposited onto or very near the mesh wires was intact, but the pores were not entirely filled in samples CM-2, CM-3, and CM-4. We attribute this to the dynamics of evaporation of ethanol from the membrane during the drying process. For CM-1, because the ethanol amount in the coating solution was the smallest (i.e., the PP-SiO_2 concentration was the highest), the slurry viscosity was relatively high, which sustained the drying solution between the meshes. In addition, this highly viscous slurry was able to resist the capillary force that would tend to pull the material back toward the wires during evaporation. Thus, no visible holes or cracks were observed in the membrane. However, with increased ethanol amount in the coating solution, as in the case of CM-2, the rate of evaporation of ethanol from the membrane increased, while the viscosity of the slurry decreased.

dx.doi.org/10.1021/la5031526 | Langmuir XXXX, XXX, XXX−XXX

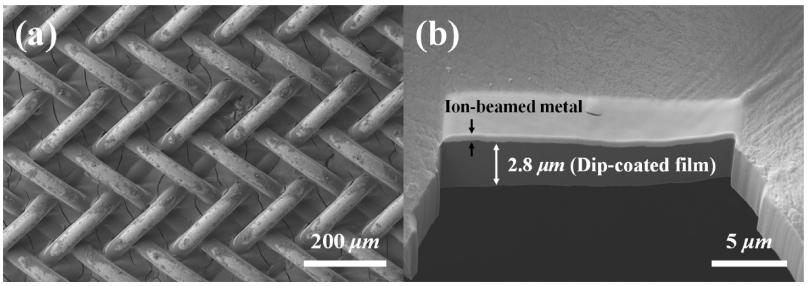

Figure 4. HRSEM images of composite membrane CM-1.

This creates higher capillary forces, combined with a decreased ability to resist deformation, ultimately resulting in the formation of holes in the membrane. This trend continues in the cases of CM-3 and CM-4 (as the ethanol concentration in the coating solution increases in both of these cases), resulting in the formation of even larger holes.

Higher magnification HRSEM imaging of slurry between stainless steel meshes was used for the detailed observation of CM-1, as shown in Figure 4. These HRSEM images show the morphology of the CM-1 membrane. Small cracks are visible in the film, which may play a role in the water permeation through the membrane (see Figure 4a). Note that they are much smaller than the "holes" that appear between the wires in the films with higher ethanol content. Figure 4b shows a cross section of the film having the thickness of approximately 2.8 μm, prepared by focused ion beam (FIB) milling. The smooth, lighter-colored part on top of the film is metal deposited to help provide a clean cross section. The cross-sectional view of the milled surface (noted as "Dip-coated film") is apparently quite smooth, indicating no visible pores (see Figure S7).

As shown in the low and high magnification transmission electron microscopy (TEM) images (Figure 5), the nanostructure of the membrane arises from the incorporation of the spherical silica nanoparticles, which are 10−25 nm in diameter.

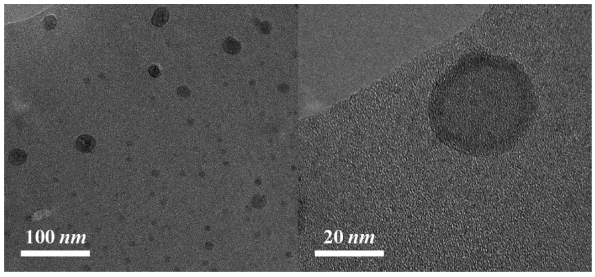

Figure 5. Low and high magnification TEM images of CM-1 membrane.

3.2. X-ray Photoelectron Spectroscopy (XPS) and Fourier Transform Infrared (FT-IR) Spectroscopy Studies.

The surface elemental composition of the CM-1 membrane was analyzed using XPS, as depicted in Figure 6a. An intense F 1s peak at 686.2 eV, a broad O 1s peak at 530.9 eV, an N 1s peak at 402.8 eV, a strong C 1s peak at 284.6 eV, and a weak Si 2p peak at 102.1 eV were evident, reflecting the constituent elements of PDDA, PFO, and silica particles used to prepare the membrane. High resolution spectra of the O 1s, C 1s, and Si 2p peaks are shown in Figure 6b−d, respectively. The C 1s peak (Figure 6c) is split into two peaks at 284.8 and 291.9 eV, which can be assigned to the $-CH_2-$ and $-CF_2-$ groups, respectively.[26]

The FT-IR spectrum of the CM-1 membrane from Figure 7 shows absorbance at 1200 cm^{-1} and a shoulder peak at 1148 cm^{-1}, which represent the C−F stretching vibration.[31] The small peak centered at 946 cm^{-1} is attributed to the presence of Si−O species.[32] The peaks observed near 1478 and at 2937 cm^{-1} can be assigned to the presence of $-CH_3$ and $-CH_2$ groups. The intense peak near 1678 cm^{-1} corresponds to C═O stretching. The FT-IR results are consistent with the XPS studies.

3.3. Wetting Behavior of the Composite Membranes.

The wetting behavior of the composite membranes was studied in detail. The uncoated stainless steel mesh was easily wetted by both water and oil. Figure 8 shows an optical image of the wetting behavior of water and hexadecane droplets on CM-1. As shown in Figure 8, the water droplet spreads out and permeates through the membrane immediately, showing the strong superhydrophilic character of CM-1, with a CA of 0°. A water droplet (~10 μL) was spread on the membranes in only ~0.6 s, which was a much shorter time than that of the original stainless steel mesh (more than 5 s). The wetting behavior of a hexadecane droplet is also shown in Figure 8. The droplet sits on the membrane surface with a macroscopic CA of 95 ± 2°, showing the oil repellent properties (oleophobic) of the membrane. CA stability is critical for extended use in applications based on wetting properties. Therefore, we also evaluated the CA variation with time to characterize the repeatability of these membranes.[33] To analyze the deterioration of the oleophobicity, we used hexadecane as the test liquid. Hexadecane droplets positioned on the composite membranes had CAs greater than 90° for over 45 min, suggesting the stability of the membranes in sustaining oleophobicity.

The composite membranes consisted of SiO_2 nanoparticles and the complex polymer PDDA and PFO. This membrane shows excellent oleophobic and hydrophilic properties because the polymers, PDDA and PFO, contain a high density of fluorinated groups, as well as carboxyl and ammonium groups. As suggested by Yang et al.,[26] the hydrophobic−oleophobic fluorinated groups may remain in a relatively mobile state at the surface of the membrane. When water contacts the membrane, the fluorinated moieties reorganize to expose the hydrophilic quaternary amine and hydroxyl groups.[26] When oil contacts the surface, the oleophobic fluorinated groups remain exposed. The inorganic silica particles are also hydrophilic, owing to the silanol groups on their surface.[34] Thus, they contribute to the film performance both by creating a nanoscale texture and by presenting hydrophilic groups. The wetting behavior of the composite membranes CM-2, CM-3, and CM-4 were also studied. These composite membranes also showed superhydrophilicity and oleophobicity; water droplets spread quickly on these membranes, while hexadecane droplets initially showed a macroscopic CA exceeding 90°. However, for CM-3 and CM-4, this was maintained for only ~2 s, and the oil spread completely within 60 s. The situation was similar for CM-2, except that it

dx.doi.org/10.1021/la5031526 | Langmuir XXXX, XXX, XXX−XXX

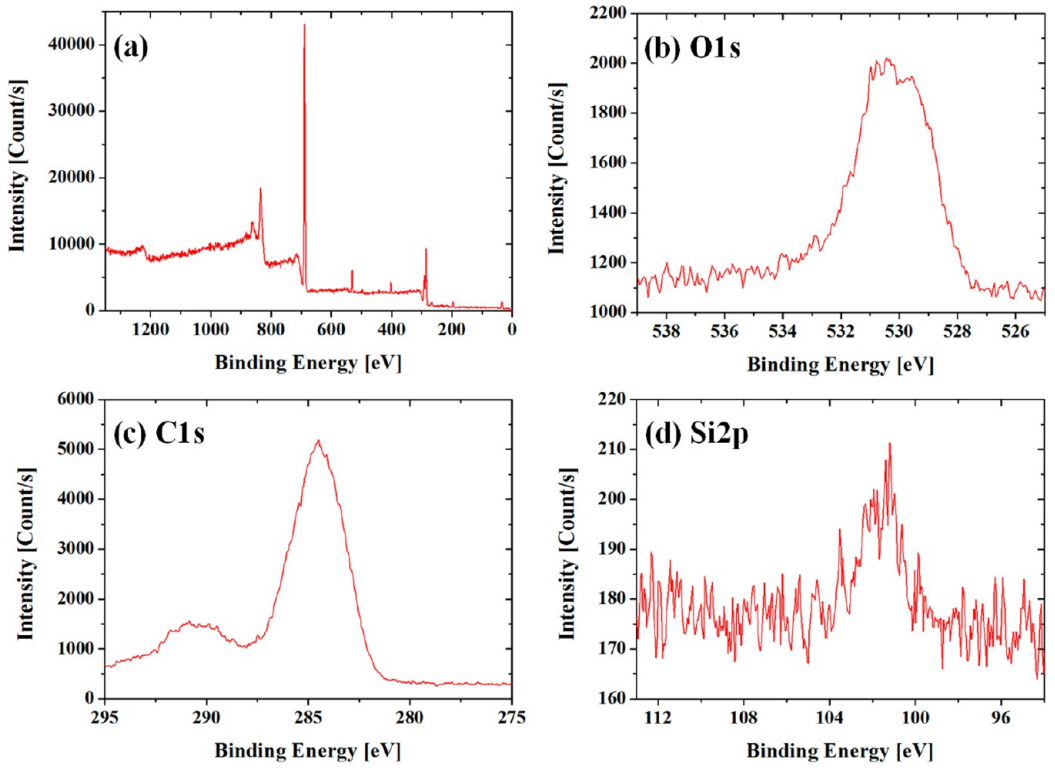

Figure 6. (a) XPS survey spetrum of the CM-1 membrane, and high resolution of (b) O 1s, (c) C 1s, and (d) Si 2p regions of the spectrum.

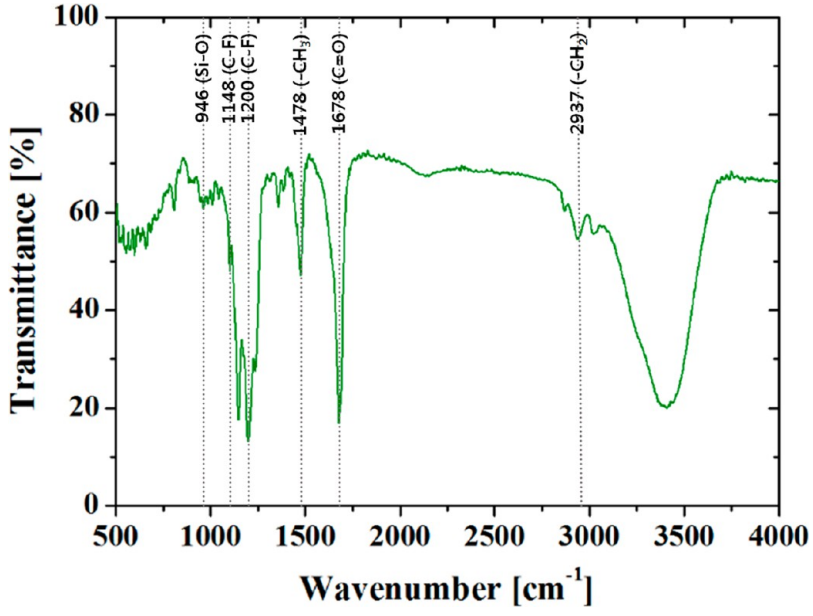

Figure 7. FT-IR spectrum of the CM-1 membrane.

maintained a final CA of ~37 ±5°. The micrometer-sized holes formed in these membranes are responsible for the decrease in the apparent macroscopic hexadecane CA with respect to time.

3.4. Oil–Water Separation by the Composite Membranes. To test the oil–water separation capability of the composite membranes, we carried out a series of proof of concept studies. The oil–water separation experiments for the composite membranes, CM-1, CM-2, CM-3, and CM-4, were performed as shown in Figure 9. Hexadecane was dyed red using Oil Red O. A 150 mL mixture of hexadecane and water (v/v: 50/100 mL) was poured onto the as-prepared composite membranes, and the permeated water was collected in the beaker underneath. In the case of CM-1 (Figure 9a), almost all the water permeated through the membrane within 12 min, leaving hexadecane on top of the membrane, demonstrating the effectiveness of this membrane for efficient oil–water separation. However, in the case of CM-2 (Figure 9b), even though all the water passed through the membrane completely, some hexadecane also passed through the membrane, providing poor oil–water separation. The CM-3 and CM-4 membranes showed very poor performance in oil–water separation because both

dx.doi.org/10.1021/la5031526 | *Langmuir* XXXX, XXX, XXX–XXX

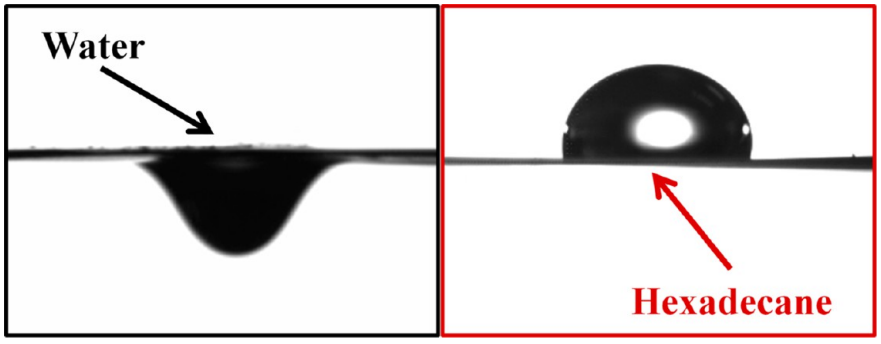

Figure 8. Optical images of wetting behavior of water and hexadecane droplets on composite membrane CM-1.

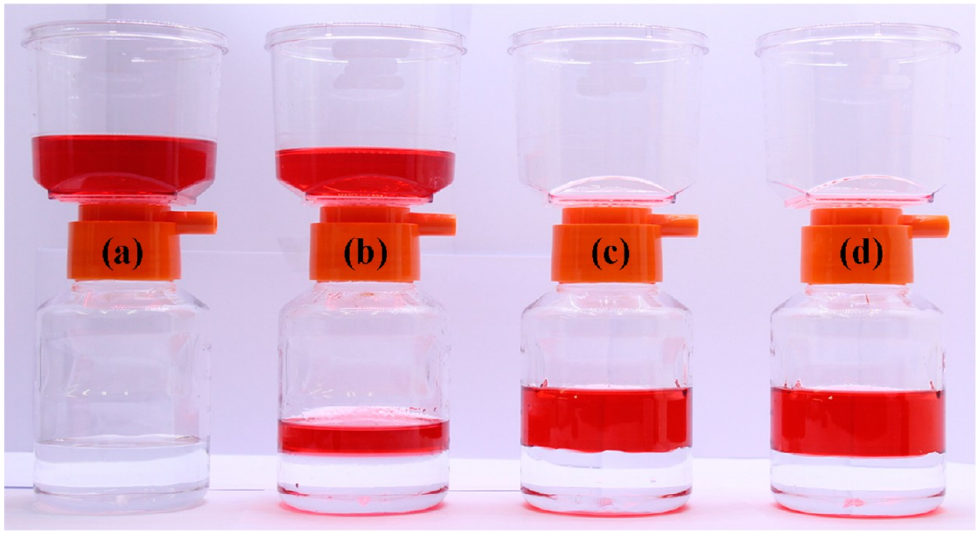

Figure 9. Oil/water separation experiment for the composite membranes: (a) CM-1, (b) CM-2, (c) CM-3, and (d) CM-4.

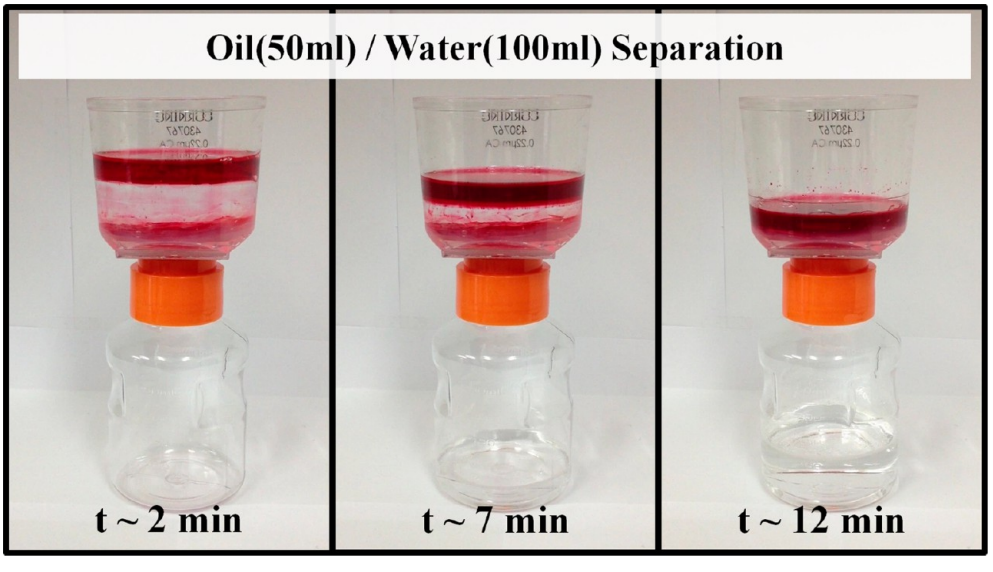

Figure 10. Detailed oil–water separation capability of composite membrane, CM-1.

hexadecane and water permeated through the membrane within 5 min.

The detailed oil–water separation capability of CM-1 is shown in Figure 10. At the beginning, 50 mL of hexadecane was poured into the beaker, the bottom of which was covered with the membrane. The oil did not penetrate the membrane. Then, 100 mL of water was poured into the beaker. Once the water in the oil–water mixture contacted the membrane, the surface started to reconfigure. Within seconds, the water started passing through the membrane, whereas the hexadecane remained above the membrane. The 100 mL of water completely penetrated through the membrane within 10 min; thus, the filter had a flow rate of

dx.doi.org/10.1021/la5031526 | *Langmuir* XXXX, XXX, XXX–XXX

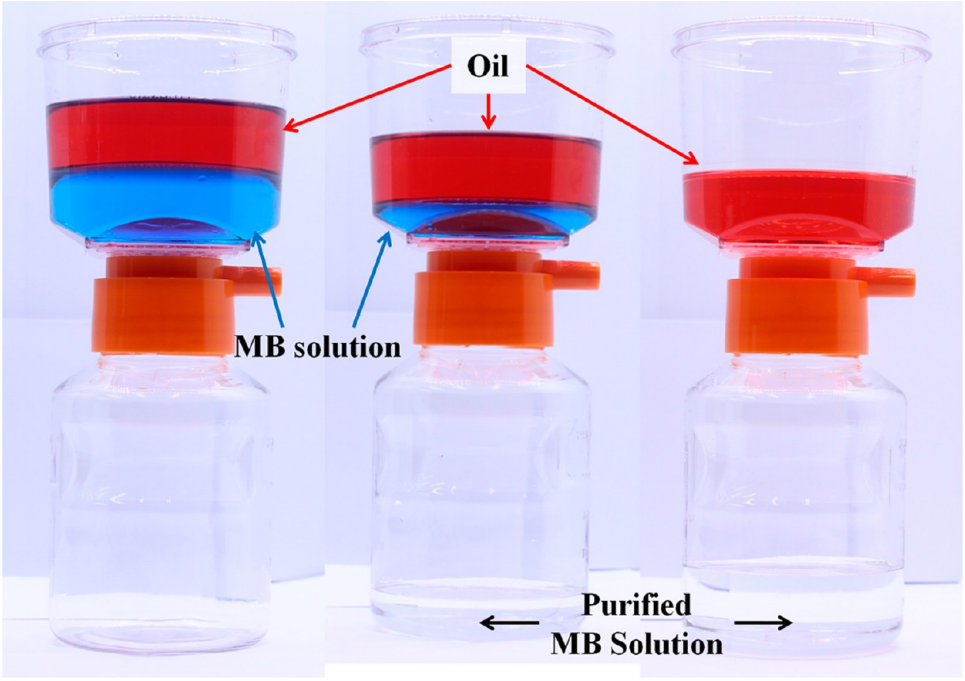

Figure 11. Detailed oil–MB separation capability as well as purification of MB by composite membrane, CM-1.

about 10 mL/min with only hydrostatic pressure due to gravity as the driving force for flow. No oil was visible in the collected water. A video illustrating the separation of oil and water is provided in the Supporting Information (Movie S1). The separation efficiency was measured as the mass of recovered water divided by the initial mass of water,[35] and was as high as 97%. Meanwhile, hexadecane remained above the membrane because of the oleophobicity and low water-adhesion properties of the membrane. This membrane could be used to separate several liters of oil–water mixtures only using gravity in a single operation. Hexadecane did not leak through the filter membrane even after 2 weeks. This demonstrates the excellent characteristics of the composite membrane as an oil–water separation filter.

The influence of repeated wetting by water on the wettability of the membrane was also investigated to evaluate its reusability, which is an important criterion for practical applications. After the first saturated adsorption of water, the membrane was dried thoroughly overnight. After each oil–water separation experiment, the hexadecane CA and the water uptake capacity was measured again. The process was repeated more than 30 times, and the influence of the repeated processes on the hexadecane CA was recorded. The coated mesh was easily cleaned for reuse. Hexadecane left on the membrane was washed away completely by water. After drying the mesh, it could be reused for oil–water separation. Thus, CM-1 retained its excellent oleophobicity even after repeated oil–water separation experiments. The oleophobic properties of the composite membrane prevented it from becoming fouled by oils, facilitating extended or repeated use of the membrane.

3.5. Water Purification by the Composite Membranes. Recently, Gupta et al.[36] reported the in situ creation of graphene-like material anchored onto the surfaces of river sand without the need of any additional binder for application in efficient water purification. Building on this idea, in another set of experiments shown in Figure 1, a graphene plug (thickness ∼2 cm) was stacked below the composite membrane, CM-1, to achieve water purification as well as oil–water separation. This assembly could efficiently separate hexadecane from an aqueous solution containing MB and also completely decolor the MB solution (Figure 11), indicating the potential of this assembly for both oil–water separation and water purification. This filter with the graphene plug had a flow rate of about 0.167 mL/min. If we assume a pressure drop of 0.005 bar (2 in. of water), then the permeability can be estimated as follows: If the diameter of the graphene plug is 21 mm, then the area is 3.5×10^{-4} m^2 and the flow rate is 0.167 mL/min = 0.01 L/h and then the permeability (in L m^{-2} h^{-1} bar^{-1}) is 29 L m^{-2} h^{-1}/0.005 bar, which is about 6000 L m^{-2} h bar^{-1}. It is reasonable that the graphene plug would make the flow much slower since its thickness is much thicker than that of the membrane.

As illustrated in Figure 10, a pressure of a few inches of water is enough to push the aqueous phase through the membrane, but not enough to cause the oil phase to penetrate. The permeability can be estimated as follows: The 18 mm diameter membrane has a surface area of 0.00025 m^2. As shown in Figure 10, 0.1 L of water permeates the membrane in about 1/6 h. The pressure varies in this gravity-driven process but is, on average, around 0.005 bar (2 in. of water). This gives an approximate permeability of 800 000 L m^{-2} h^{-1} bar^{-1} under these conditions, which is suitable for gravity-driven separation at reasonable flow rates.

Figure 12 shows the decolorization of MB as reflected by the absorption spectra before and after filtration. Clearly, the removal of MB molecules from the solution by the graphene plug was efficient, mainly owing to its giant π-conjugation system and two-dimensional planar structure. Graphene is particularly effective for adsorbing aromatic molecules because of the strong $\pi-\pi$ interactions of aromatic rings with graphene. Aromatics are of particular importance because they often have high visibility, odor, or toxicity at low concentrations (for example, the dye used in this study is visible at low concentrations, polychlorinated biphenyl molecules (PCBs) are persistent organic pollutants of great concern). The MB molecules are expected to adsorb on the surface of the graphene sheets with an offset face-to-face

dx.doi.org/10.1021/la5031526 | *Langmuir* XXXX, XXX, XXX–XXX

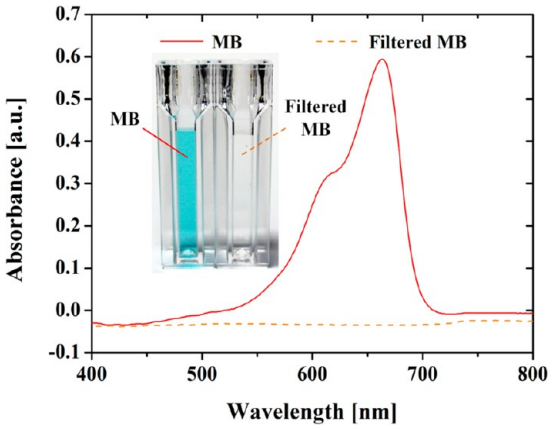

Figure 12. Removal of MB by composite membrane, CM-1, in terms of absorption spectra.

orientation by $\pi-\pi$ stacking interactions, during which external mass transfer between the MB solution and the graphene sheets together with boundary layer diffusion occurs.[37]

4. CONCLUSION

We developed and demonstrated a simple dip-coating approach that requires no post-treatment steps to synthesize a composite membrane with excellent oleophobic and superhydrophilic properties. The fabrication technique is simple and readily scalable for mass production. Water was quickly and selectively removed from oil by the composite membrane, which had the additional capacity for water purification. We expect that our oil–water separation methodology using a novel oleophobic–superhydrophilic composite membrane will have numerous applications, including the cleanup of oil spills, wastewater treatment, and fuel purification.

■ ASSOCIATED CONTENT

Supporting Information

Gravity-driven hybrid membrane for oleophobic–superhydrophilic oil–water separation and water purification by graphene. This material is available free of charge via the Internet at http://pubs.acs.org.

■ AUTHOR INFORMATION

Corresponding Author

*Tel: +82-2-3290-3376. E-mail: skyoon@korea.ac.kr.

Notes

The authors declare no competing financial interest.

■ ACKNOWLEDGMENTS

This work was supported by a Center for Inorganic Photovoltaic Materials (No. 2012-0001169) grant funded by the Korea government (MSIP), NRF-2013R1A2A2A05005589, and the Industrial Strategic Technology Development Program (MKE 10045221). This work was also supported by the Global Frontier R&D Program (2013M3A6B1078879) of Center for Hybrid Interface Materials (HIM) funded by the Ministry of Science, ICT & Future Planning. This work was supported by a grant from the New & Renewable Energy of the Korea Institute of Energy Technology Evaluation and Planning (KETEP) funded by the Korea government Ministry of Knowledge Economy (No. 20133030010890). The Authors extend their appreciation to the Deanship of Scientific Research at King Saud University for funding the work through the research group project No. RGP-089

■ REFERENCES

(1) Yuan, J.; Liu, X.; Akbulut, O.; Hu, J.; Suib, S. L.; Kong, J.; Stellacci, F. Superwetting nanowire membranes for selective absorption. *Nat. Nanotechnol.* **2008**, *3*, 332–336.

(2) Shannon, M. A.; Bohn, P. W.; Elimelech, M.; Georgiadis, J. G.; Mariñas, B. J.; Mayes, A. M. Science and technology for water purification in the coming decades. *Nature* **2008**, *452*, 301–310.

(3) Arbatan, T.; Fang, X.; Shen, W. Superhydrophobic and oleophilic calcium carbonate powder as a selective oil sorbent with potential use in oil spill clean-ups. *Chem. Eng. J.* **2011**, *166*, 787–791.

(4) Karakasi, O.; Moutsatsou, A. Surface modification of high calcium fly ash for its application in oil spill clean up. *Fuel* **2010**, *89*, 3966–3970.

(5) Choi, H. M.; Cloud, R. M. Natural sorbents in oil spill cleanup. *Environ. Sci. Technol.* **1992**, *26*, 772–776.

(6) Teas, C.; Kalligeros, S.; Zanikos, F.; Stournas, S.; Lois, E.; Anastopoulos, G. Investigation of the effectiveness of absorbent materials in oil spills clean up. *Desalination* **2001**, *140*, 259–264.

(7) Inagaki, M.; Kawahara, A.; Konno, H. Sorption and recovery of heavy oils using carbonized fir fibers and recycling. *Carbon* **2002**, *40*, 105–111.

(8) Deschamps, G.; Caruel, H.; Borredon, M.-E.; Bonnin, C.; Vignoles, C. Oil removal from water by selective sorption on hydrophobic cotton fibers. 1. Study of sorption properties and comparison with other cotton fiber-based sorbents. *Environ. Sci. Technol.* **2003**, *37*, 1013–1015.

(9) Sun, X.-F.; Sun, R.; Sun, J. A convenient acetylation of sugarcane bagasse using NBS as a catalyst for the preparation of oil sorption-active materials. *J. Mater. Sci.* **2003**, *38*, 3915–3923.

(10) Cheryan, M.; Rajagopalan, N. Membrane processing of oily streams. Wastewater treatment and waste reduction. *J. Membr. Sci.* **1998**, *151*, 13–28.

(11) Al-Shamrani, A.; James, A.; Xiao, H. Destabilisation of oil–water emulsions and separation by dissolved air flotation. *Water Res.* **2002**, *36*, 1503–1512.

(12) Rubio, J.; Souza, M.; Smith, R. Overview of flotation as a wastewater treatment technique. *Miner. Eng.* **2002**, *15*, 139–155.

(13) Wang, L.; Zhang, X.; Li, B.; Sun, P.; Yang, J.; Xu, H.; Liu, Y. Superhydrophobic and ultraviolet-blocking cotton textiles. *ACS Appl. Mater. Interfaces* **2011**, *3*, 1277–1281.

(14) Lee, C. H.; Johnson, N.; Drelich, J.; Yap, Y. K. The performance of superhydrophobic and superoleophilic carbon nanotube meshes in water–oil filtration. *Carbon* **2011**, *49*, 669–676.

(15) Li, A.; Sun, H.-X.; Tan, D.-Z.; Fan, W.-J.; Wen, S.-H.; Qing, X.-J.; Li, G.-X.; Li, S.-Y.; Deng, W.-Q. Superhydrophobic conjugated microporous polymers for separation and adsorption. *Energy Environ. Sci.* **2011**, *4*, 2062–2065.

(16) Liang, H. W.; Guan, Q. F.; Chen, L. F.; Zhu, Z.; Zhang, W. J.; Yu, S. H. Macroscopic-scale template synthesis of robust carbonaceous nanofiber hydrogels and aerogels and their applications. *Angew. Chem., Int. Ed.* **2012**, *51*, 5101–5105.

(17) Gui, X.; Wei, J.; Wang, K.; Cao, A.; Zhu, H.; Jia, Y.; Shu, Q.; Wu, D. Carbon nanotube sponges. *Adv. Mater.* **2010**, *22*, 617–621.

(18) Zhang, J.; Seeger, S. Polyester materials with superwetting silicone nanofilaments for oil/water separation and selective oil absorption. *Adv. Funct. Mater.* **2011**, *21*, 4699–4704.

(19) Wei, Q.; Mather, R.; Fotheringham, A.; Yang, R. Evaluation of nonwoven polypropylene oil sorbents in marine oil-spill recovery. *Mar. Pollut. Bull.* **2003**, *46*, 780–783.

(20) Kulawardana, E. U.; Neckers, D. C. Photoresponsive oil sorbers. *J. Polym. Sci., Part A: Polym. Chem.* **2010**, *48*, 55–62.

(21) Jin, M.; Wang, J.; Yao, X.; Liao, M.; Zhao, Y.; Jiang, L. Underwater oil capture by a three-dimensional network architectured organosilane surface. *Adv. Mater.* **2011**, *23*, 2861–2864.

(22) Xue, Z.; Wang, S.; Lin, L.; Chen, L.; Liu, M.; Feng, L.; Jiang, L. A novel superhydrophilic and underwater superoleophobic hydrogel-coated mesh for oil/water separation. *Adv. Mater.* **2011**, *23*, 4270–4273.

(23) Nosonovsky, M.; Bhushan, B. Multiscale effects and capillary interactions in functional biomimetic surfaces for energy conversion and green engineering. *Philos. Trans. R. Soc., A* **2009**, *367*, 1511−1539.
(24) Jung, Y. C.; Bhushan, B. Wetting behavior of water and oil droplets in three-phase interfaces for hydrophobicity/philicity and oleophobicity/philicity. *Langmuir* **2009**, *25*, 14165−14173.
(25) Liu, M.; Wang, S.; Wei, Z.; Song, Y.; Jiang, L. Bioinspired design of a superoleophobic and low adhesive water/solid interface. *Adv. Mater.* **2009**, *21*, 665−669.
(26) Yang, J.; Zhang, Z.; Xu, X.; Zhu, X.; Men, X.; Zhou, X. Superhydrophilic−superoleophobic coatings. *J. Mater. Chem.* **2012**, *22*, 2834.
(27) Zhang, L.; Zhang, Z.; Wang, P. Smart surfaces with switchable superoleophilicity and superoleophobicity in aqueous media: toward controllable oil/water separation. *NPG Asia Mater.* **2012**, *4*, e8.
(28) Novoselov, K. S.; Geim, A. K.; Morozov, S.; Jiang, D.; Zhang, Y.; Dubonos, S.; Grigorieva, I.; Firsov, A. Electric field effect in atomically thin carbon films. *Science* **2004**, *306*, 666−669.
(29) Kemp, K. C.; Seema, H.; Saleh, M.; Mahesh, K.; Chandra, V.; Kim, K. S. Environmental applications using graphene composites: Water remediation and gas adsorption. *Nanoscale* **2013**, *5*, 3149−3171.
(30) Guo, J.; Wang, R.; Tjiu, W. W.; Pan, J.; Liu, T. Synthesis of Fe nanoparticles@ graphene composites for environmental applications. *J. Hazard. Mater.* **2012**, *225*, 63−73.
(31) Huang, X.; Zacharia, N. Surfactant co-assembly and ion exchange to modulate polyelectrolyte multilayer wettability. *Soft Matter* **2013**, *9*, 7735.
(32) Almedia, R. M.; Pantano, C.G. Structural investigation of silica gel films by infrared spectroscopy. *J. Appl. Phys.* **1990**, *68*, 4225−4232.
(33) Boinovich, L. B.; Emelyanenko, A. M.; Pashinin, A. S.; Lee, C. H.; Drelich, J.; Yap, Y. K. Origins of thermodynamically stable superhydrophobicity of boron nitride nanotubes coatings. *Langmuir* **2011**, *28*, 1206−1216.
(34) Dolatzadeh, F.; Jalili, M.; Moradian, S. Influence of various loadings of hydrophilic or hydrophobic silica nanoparticles on water uptake and porosity of a polyurethane coating. *Mater. Corros.* **2012**, *63*, 9999.
(35) Pan, Q.; Wang, M.; Wang, H. Separating small amount of water and hydrophobic solvents by novel superhydrophobic copper meshes. *Appl. Surf. Sci.* **2008**, *254*, 6002−6006.
(36) Gupta, S. S.; Sreeprasad, T. S.; Maliyekkal, S. M.; Das, S. K.; Pradeep, T. Graphene from sugar and its application in water purification. *ACS Appl. Mater. Interfaces* **2012**, *4*, 4156−4163.
(37) Rodríguez, A.; García, J.; Ovejero, G.; Mestanza, M. Adsorption of anionic and cationic dyes on activated carbon from aqueous solutions: equilibrium and kinetics. *J. Hazard. Mater.* **2009**, *172*, 1311−1320.